

Nonasymptotic Convergence Rates for Plug-and-Play Methods With MMSE Denoisers

Henry Pritchard and Rahul Parhi, *Member, IEEE*

Abstract—It is known that the minimum-mean-squared-error (MMSE) denoiser under Gaussian noise can be written as a proximal operator, which suffices for asymptotic convergence of plug-and-play (PnP) methods but does not reveal the structure of the induced regularizer or give convergence rates. We show that the MMSE denoiser corresponds to a regularizer that can be written explicitly as an upper Moreau envelope of the negative log-marginal density, which in turn implies that the regularizer is 1-weakly convex. Using this property, we derive (to the best of our knowledge) the first sublinear convergence guarantee for PnP proximal gradient descent with an MMSE denoiser. We validate the theory with a one-dimensional synthetic study that recovers the implicit regularizer. We also validate the theory with imaging experiments (deblurring and computed tomography), which exhibit the predicted sublinear behavior.

I. BACKGROUND

In this work, we focus on the setting of *linear inverse problems*, where $x \in \mathbb{R}^n$ is the true signal, $y \in \mathbb{R}^m$ is the observed signal obtained by

$$y = Ax + \epsilon, \quad (1)$$

for linear *forward operator* $A \in \mathbb{R}^{m \times n}$ and measurement noise $\epsilon \sim \mathcal{N}(0, \sigma^2 I)$. The task of recovering x from y is extensively studied in statistics and signal processing. A special case is the denoising problem, obtained when $A = I$:

$$z = x + \epsilon. \quad (2)$$

Although simpler, denoising is directly useful in solving general inverse problems, often as an intermediate step.

Recovering x from y is often posed as the minimization of a regularized objective function

$$F(x) := f(x) + g(x), \quad (3)$$

where f is a data-fidelity term (typically $f(x) := \frac{1}{2} \|Ax - y\|^2$ under Gaussian noise), and g is a regularization term that encodes prior beliefs about the *class of admissible solutions*. For instance, the ℓ^1 -norm ($g(x) \propto \|x\|_1$) promotes sparsity and underlies the theory of compressed sensing [6], [9], [17]. Similarly, total variation (TV), defined as $g(x) \propto \text{TV}(x) := \sum_k |x_k - x_{k-1}|$ favors piecewise-constant solutions and is widely used in image denoising [10], [11], [36], [44], [52]. More recently, much of research in imaging inverse problems has shifted towards *learned regularizers* [18], [19], [22], [24], [29], [33], [43], [48]. Without regularization, the problem is often *ill-posed* in the sense of Hadamard [21], [28]: Solutions

may be non-unique, unstable, or nonexistent. Since the data-fidelity term is typically well-behaved, the regularizer largely determines the structure of solutions. More broadly, the regularizer largely dictates how optimization algorithms behave, so understanding its structure is crucial.

A. Proximal Gradient Descent.

Gradient descent is a classical method for minimizing smooth (Lipschitz gradient) objective functions, with iterations

$$x_{k+1} \leftarrow x_k - \gamma \nabla F(x_k). \quad (4)$$

With appropriately chosen step size $\gamma > 0$, the iterates x_k converge to a stationary point [32]. However, gradient descent is not well-suited for nonsmooth objectives.

Proximal gradient descent (PGD) addresses this limitation by splitting the objective function as in (3). The data-fidelity term f is typically smooth while the regularizer g is often not (such as ℓ^1 or TV). At each iteration, PGD takes a gradient step on the data-fidelity term followed by a *proximal step* for the regularizer, yielding iterations of the form

$$x_{k+1} \leftarrow \text{prox}_{\gamma g}(x_k - \gamma \nabla f(x)). \quad (5)$$

Here $\text{prox}_{\gamma g}$ denotes the proximal operator of g (see Definition II.6), originally introduced by Moreau in [40]. Convergence of PGD has been widely studied in both convex and non-convex settings and can be established under various assumptions on f and g with appropriately chosen step sizes $\gamma > 0$ [35, Table 1].

B. Plug-and-Play Methods

The *plug-and-play* (PnP) framework [33], [58] extends PGD by replacing the proximal step $\text{prox}_{\gamma g}$ with a generic denoiser D_σ [7]. This substitution is motivated by the interpretation of $\text{prox}_{\gamma g}$ as the maximum a posteriori (MAP) solution to the denoising problem (2) under prior $p_X \propto e^{-\gamma g}$ [14, Eq. (10.13)], the exact problem denoisers are designed to solve. The PnP iteration is given by

$$x_{k+1} \leftarrow D_\sigma(x_k - \gamma \nabla f(x_k)), \quad (6)$$

and has been shown to yield state-of-the-art results when combined with powerful image denoisers such as BM3D [16] or a deep neural network (DNN) [31], [60]. Often, we use data fidelity term $f(x) := \frac{1}{2} \|Ax - y\|^2$, in which case the PnP iteration becomes

$$x_{k+1} \leftarrow D_\sigma(x_k - \gamma A^T A(x_k - y)). \quad (7)$$

A central challenge in the PnP framework is that while a proximal operator is always tied to a well-defined regularizer,

The authors are with the Department of Electrical and Computer Engineering, University of California, San Diego (e-mail: hepritchard@ucsd.edu; rahul@ucsd.edu).

many of the most effective denoising methods are not. This substitution therefore breaks the direct connection to an explicit optimization problem, making theoretical interpretations and convergence claims difficult. Much of the literature imposes strict assumptions on the denoiser to obtain convergence guarantees. Many of the most effective denoisers do not satisfy these assumptions, yet still achieve excellent results (for example [1]).

C. Related Works.

When f and g are convex with L -smooth f , it is well known that PGD converges to a fixed point for appropriate step size γ [45, Section 4.2]. This result can be proven via the machinery of monotone operator theory, the goal being to show that the composite PGD step (5) constitutes an averaged operator, guaranteeing convergence [3], [13], [15].¹

In particular, convergence of PnP-PGD has been shown under tight assumptions on the denoiser, such as averaged/nonexpansive behavior [56] or suitable Lipschitz (e.g., residual-Lipschitz) bounds [53]. Many works impose these assumptions through architectural constraints on the learned denoisers via, e.g., spectral normalization [53] or through explicit training techniques [8], [57]. In [47], the authors propose a technique for learning a maximally monotone operator. Convergence of PnP has also been shown for specific denoisers, such as kernel denoisers [23], denoisers that can be written as the gradient step of a smooth function [30], bounded denoisers [12], and linear denoisers [42].

Instead of treating the denoiser as a black box with certain conditions, a complementary line of work leverages its intrinsic *statistical* structure. The MMSE estimator under Gaussian noise is a notable example. With the Tweedie/Stein identities [20], [55], the MMSE denoiser can be tied to the score function, endowing it with useful structural properties [38]. Further, [25] and [27] showed that the MMSE denoiser is C^∞ and can be written as the proximal map of a regularizer (which is C^∞) under various forward and noise models, and derived an explicit formula for this regularizer (28). This progress enabled the derivation of asymptotic convergence for both the ADMM [46] and PGD [59] variants of PnP using an MMSE denoiser. However, a gap in the theory remains: The explicit formula offers little insight into the behavior of the induced regularizer, and there are no *nonasymptotic* convergence rates tailored to MMSE denoisers.

D. Contributions.

We make the following contributions.

- **Characterization of the implicit regularizer of the MMSE denoiser.** We show in Theorem III.2 that the MMSE denoiser is the proximal map of a regularizer that admits an explicit form as an *upper Moreau envelope*, i.e., $\phi_{\text{MMSE}}(x)$ is, up to a constant,

$$\sigma^2 \sup_z (f_Z(z) - \frac{1}{2\sigma^2} \|z - x\|^2) \quad (8)$$

¹When g is proper, lower-semicontinuous, convex, ∂g is maximally monotone, making $\text{prox}_{\gamma g} = (I + \gamma \partial g)^{-1}$ firmly-nonexpansive, i.e., $1/2$ -averaged. The gradient step is also averaged for L -smooth f , making their composition an averaged operator.

where $f_Z = -\log p_Z$ is the negative log marginal distribution in the noise model (2). This is an explicit *and* interpretable description of the regularizer implicit in the MMSE denoiser, and we believe that this identity is new.

- **Nonasymptotic convergence of MMSE-PGD via weak convexity.** In Corollary III.3, we prove that $x \mapsto \phi_{\text{MMSE}}(x) + \frac{1}{2} \|x\|^2$ is convex, hence ϕ_{MMSE} is 1-weakly convex. With this property we establish (to the best of our knowledge) the first *nonasymptotic* convergence guarantees for PGD-PnP with an MMSE denoiser in Theorem III.6. In particular, we show that, under an L -smooth data-fidelity term f with $L < 1$, PGD reaches an $\mathcal{O}(1/\sqrt{k})$ -stationary point after k iterations.
- **Experiments.** In Section IV, we consider the following experimental setups: (i) A one-dimensional synthetic example validating the upper Moreau envelope form of the regularizer implicit in the MMSE denoiser by comparing a learned DNN estimator to its explicit form, (ii) Gaussian deblurring on the MNIST dataset [34], and (iii) computed tomography on the MayoCT dataset [37]. In both imaging tasks we observe the predicted sublinear $\mathcal{O}(1/\sqrt{k})$ convergence in the subgradient residual.

II. PRELIMINARIES

In this section, we collect some definitions and results used in the remainder of the paper. First, we recall the definition of the *convex conjugate*, also known as the Legendre-Fenchel transform or Fenchel conjugate. See for example [51].

Definition II.1. For a function $f : \mathbb{R}^n \rightarrow \mathbb{R}$, the convex conjugate f^* is given by

$$f^*(x) := \sup_{y \in \mathbb{R}^n} \{ \langle x, y \rangle - f(y) \}. \quad (9)$$

Definition II.2 (Lower Moreau Envelope). Let $f : \mathbb{R}^n \rightarrow \mathbb{R}$ be a function with $\gamma > 0$. The *lower Moreau envelope* of f is given by

$$M_\gamma f(x) := \inf_y \left(f(y) + \frac{1}{2\gamma} \|y - x\|^2 \right). \quad (10)$$

Definition II.3 (Upper Moreau Envelope). Let $f : \mathbb{R}^n \rightarrow \mathbb{R}$ be a function with $\gamma > 0$. The *upper Moreau envelope* of f is given by

$$M^\gamma f(x) := \sup_y \left(f(y) - \frac{1}{2\gamma} \|y - x\|^2 \right). \quad (11)$$

Note that the lower Moreau envelope is the usual Moreau envelope, but we make the distinction in this paper since we use both lower and upper Moreau envelopes. For the infimum defining the lower Moreau envelope to be achieved, f must be lower-semicontinuous. An important property of the lower Moreau envelope $M_\gamma f$ is that it shares global minimizers with f whenever f is lower-semicontinuous, i.e. $\arg \min_x f(x) = \arg \min_x M_\gamma f(x)$. See [4] for further background.

Definition II.4 (Weak convexity). Let $f : \mathbb{R}^n \rightarrow \mathbb{R}$, $\gamma > 0$. f is called *γ -weakly convex* if the mapping $x \mapsto f(x) + \frac{\gamma}{2} \|x\|^2$ is convex.

Crucial to our analysis is the following lemma, where we include a short proof for completeness since the proof in the original reference had typos.

Lemma II.5 ([4, Lemma 3]). *If $f : \mathbb{R}^n \rightarrow \mathbb{R}$ is locally bounded, $M^\gamma M_\gamma f(x) \leq f(x)$, and equality holds if and only if f is $\frac{1}{\gamma}$ -weakly convex.*

Proof. From the definition,

$$\begin{aligned} & M^\gamma M_\gamma f(x) \\ &= \sup_y \inf_z \left(f(z) + \frac{1}{2\gamma} \|z - y\|^2 - \frac{1}{2\gamma} \|y - x\|^2 \right) \\ &\leq \sup_y f(x) = f(x), \end{aligned} \quad (12)$$

by taking $z = x$. We now write

$$\begin{aligned} & M^\gamma M_\gamma f(x) + \frac{1}{2\gamma} \|x\|^2 \\ &= \sup_y \inf_z \left(\underbrace{f(z) + \frac{1}{2\gamma} \|z\|^2}_{=: g(z)} + \frac{1}{\gamma} \langle y, x - z \rangle \right) \end{aligned} \quad (13)$$

The convex conjugate g^* evaluated at y/γ can be written as

$$\begin{aligned} g^*(y/\gamma) &= \sup_z (\langle y/\gamma, z \rangle - g(z)) \\ &= - \inf_z (g(z) - \langle y/\gamma, z \rangle), \end{aligned} \quad (14)$$

so that (13) can be written as

$$\begin{aligned} & \sup_y (-g^*(y/\gamma) + \langle y/\gamma, x \rangle) \\ &= \sup_y (\langle y, x \rangle - g^*(y)) = g^{**}(x). \end{aligned} \quad (15)$$

Therefore, we have

$$M^\gamma M_\gamma f(x) + \frac{1}{2\gamma} \|x\|^2 = \left(f + \frac{1}{2\gamma} \|\cdot\|^2 \right)^{**}(x), \quad (16)$$

and the result follows when we recall that a function equals its biconjugate if and only if it is convex [50, Section 12.2]. \square

We now turn to the proximal operator, a central tool in optimization. We will later show that MMSE estimators themselves admit a proximal representation.

Definition II.6 (Proximal operator). Let $\gamma > 0$, and $f : \mathbb{R}^n \rightarrow \mathbb{R} \cup \{+\infty\}$ be proper and lower-semicontinuous. The *proximal operator* of f with parameter γ is the mapping

$$\text{prox}_{\gamma f}(x) := \arg \min_{z \in \mathbb{R}^n} \left\{ f(z) + \frac{1}{2\gamma} \|z - x\|^2 \right\}. \quad (17)$$

Note that $\text{prox}_{\gamma f}$ is often set-valued. By coercivity of the quadratic term, $\text{prox}_{\gamma f}(x)$ is non-empty for every $x \in \mathbb{R}^n$. For a proper, lower-semicontinuous function $f : \mathbb{R}^n \rightarrow \mathbb{R} \cup \{+\infty\}$, the infimum defining the lower Moreau envelope is attained at every minimizer of the proximal problem; that is,

$$M_\gamma f(x) = f(z) + \frac{1}{2\gamma} \|x - z\|^2, \quad \forall z \in \text{prox}_{\gamma f}(x), \quad (18)$$

for all $x \in \mathbb{R}^n$. When f is a convex, lower-semicontinuous proper function, it is well known that $\text{prox}_{\gamma f}$ and $M_\gamma f$ are also related by the following formula due to Moreau [41]:

$$\nabla M_\gamma f(x) = \frac{1}{\gamma} (x - \text{prox}_{\gamma f}(x)). \quad (19)$$

Although the proximal operator of a non-convex function is generally set-valued, when $\text{prox}_{\gamma f}$ is an MMSE denoiser, it is always single-valued and continuous, which is the setting of our main results. This motivates the following extension of the Moreau gradient identity.

Theorem II.7 (Extension of the Moreau Gradient Identity). *Let $f : \mathbb{R}^n \rightarrow \mathbb{R} \cup \{+\infty\}$ be proper and lower-semicontinuous. If $\text{prox}_{\gamma f}(x)$ is single-valued and continuous for all x , then the gradient of the lower Moreau envelope exists and takes the form*

$$\nabla M_\gamma f(x) = \frac{1}{\gamma} (x - \text{prox}_{\gamma f}(x)), \quad x \in \mathbb{R}^n. \quad (20)$$

Proof. Let $h(x, z) := f(z) + \frac{1}{2\gamma} \|z - x\|^2$. We have for all $z \in \mathbb{R}^n$, $t \in \mathbb{R}$,

$$h(x + tu, z) - h(x, z) = \frac{t}{\gamma} \langle x - z, u \rangle + \frac{t^2}{2\gamma} \|u\|^2. \quad (21)$$

From the definition, $M_\gamma f(x) = \min_z h(x, z)$. Fix some $\bar{x} \in \mathbb{R}^n$ where there is a unique minimizer $\{\bar{z}\} = \text{prox}_{\gamma f}(\bar{x})$ by assumption. Take some $u \in \mathbb{R}^n$. There is some $\{z_t\} = \text{prox}_{\gamma f}(\bar{x} + tu)$ so that

$$\begin{aligned} M_\gamma f(\bar{x} + tu) &= h(\bar{x} + tu, z_t) \\ &= h(\bar{x}, z_t) + \frac{t}{\gamma} \langle \bar{x} - z_t, u \rangle + \frac{t^2}{2\gamma} \|u\|^2 \\ &\geq M_\gamma f(\bar{x}) + \frac{t}{\gamma} \langle \bar{x} - z_t, u \rangle + \frac{t^2}{2\gamma} \|u\|^2. \end{aligned} \quad (22)$$

Subtracting and dividing through by t , we get

$$\begin{aligned} & \liminf_{t \rightarrow 0} \frac{M_\gamma f(\bar{x} + tu) - M_\gamma f(\bar{x})}{t} \\ &\geq \liminf_{t \rightarrow 0} \left(\frac{1}{\gamma} \langle \bar{x} - z_t, u \rangle + \frac{t}{2\gamma} \|u\|^2 \right) \\ &= \frac{1}{\gamma} \langle \bar{x} - \bar{z}, u \rangle, \end{aligned} \quad (23)$$

where the last equality is by the assumption that $\text{prox}_{\gamma f}$ is continuous. Next,

$$\begin{aligned} M_\gamma f(\bar{x} + tu) &\leq h(\bar{x} + tu, \bar{z}) \\ &= M_\gamma f(\bar{x}) + \frac{t}{\gamma} \langle \bar{x} - \bar{z}, u \rangle + \frac{t^2}{2\gamma} \|u\|^2. \end{aligned} \quad (24)$$

Again, subtracting and dividing through by t ,

$$\begin{aligned} & \limsup_{t \rightarrow 0} \frac{M_\gamma f(\bar{x} + tu) - M_\gamma f(\bar{x})}{t} \\ &\leq \limsup_{t \rightarrow 0} \left(\frac{1}{\gamma} \langle \bar{x} - \bar{z}, u \rangle + \frac{t}{2\gamma} \|u\|^2 \right) \\ &= \frac{1}{\gamma} \langle \bar{x} - \bar{z}, u \rangle. \end{aligned} \quad (25)$$

Combining (23) and (25), we have that the directional derivative of $M_\gamma f$ at \bar{x} in direction u satisfies $\nabla_u M_\gamma f(\bar{x}) = \frac{1}{\gamma} \langle \bar{x} - \bar{z}, u \rangle$. Therefore, the gradient is

$$\nabla M_\gamma f(x) = \frac{1}{\gamma} (\bar{x} - \bar{z}) = \frac{1}{\gamma} (\bar{x} - \text{prox}_{\gamma f}(\bar{x})). \quad (26)$$

\square

Many similar versions of this identity are well known in the literature. To our knowledge, this exact formulation has not been explicitly stated.

We next review key results on MMSE denoisers and state their connection to proximal mappings, beginning with Tweedie's formula.

Theorem II.8 (Tweedie’s Formula). *Let $X \sim p_X$, $\epsilon \sim \mathcal{N}(0, \sigma^2 I)$ be independent random variables in \mathbb{R}^n , and let $Z = X + \epsilon$, $\psi_\sigma(z) := \mathbb{E}[X|Z = z]$. Then,*

$$\psi_\sigma(z) = z + \sigma^2 \nabla \log p_Z(z), \quad (27)$$

where $p_Z = p_X * \mathcal{N}(0, \sigma^2 I)$.

For a thorough introduction to Tweedie’s formula, we refer the reader to [20]. Note that Tweedie’s Formula makes no assumptions on the prior density p_X , which may even include discrete atoms.

Theorem II.9 ([27] and [25, Corollary 1]). *Let $X \sim p_X$ and $\epsilon \sim \mathcal{N}(0, \sigma^2 I)$ be independent random variables in \mathbb{R}^n , and let $Z = X + \epsilon$. Assume p_X is non-degenerate.² The MMSE estimator under (2) given by $\psi_\sigma(z) := \mathbb{E}[X|Z = z]$ has the following properties:*

- 1) *It is one-to-one from \mathbb{R}^n onto its image.*
- 2) *It is C^∞ , and so is its inverse.*
- 3) *It can be written as $\psi_\sigma(z) = \text{prox}_{\phi_{\text{MMSE}}}(z)$, where*

$$\phi_{\text{MMSE}}(z) := \begin{cases} -\frac{1}{2} \|\psi_\sigma^{-1}(z) - z\|^2 + f_Z(\psi_\sigma^{-1}(z)), & z \in \psi_\sigma(\mathbb{R}^n), \\ +\infty, & \text{otherwise,} \end{cases} \quad (28)$$

where $f_Z = -\log p_Z$.

- 4) ϕ_{MMSE} is C^∞ .

III. MAIN RESULTS

In this section, we present our theoretical contributions. We begin by introducing a new structural representation of the implicit regularizer underlying the MMSE denoiser. This characterization provides greater interpretability and serves as the foundation for deriving novel nonasymptotic convergence guarantees.

A. A New Characterization of the MMSE Regularizer.

It is known (Theorem II.9) that the MMSE denoiser is the proximal map of an infinitely differentiable penalty. Yet beyond this, the structure of the associated penalty ϕ_{MMSE} remains unclear. The only known explicit expression of ϕ_{MMSE} (28) is cumbersome and offers little analytical insight. In this section, we show that ϕ_{MMSE} admits an upper Moreau envelope representation in terms of f_Z , yielding useful insights, namely 1-weak convexity, which we will leverage to prove stronger convergence results for the PGD using an MMSE denoiser.

For the following, we will assume the setting of the denoising problem (2), letting $X \sim p_X$, $\epsilon \sim \mathcal{N}(0, \sigma^2 I)$ be independent random variables in \mathbb{R}^n , $Z = X + \epsilon$, so that $p_Z = p_X * \mathcal{N}(0, \sigma^2 I)$. We will let $f_Z := -\log p_Z$.

Lemma III.1. *The negative log marginal distribution from the denoising problem (2) can be written as*

$$f_Z = \frac{1}{\sigma^2} M_1 \phi_{\text{MMSE}} + C_{x_0}, \quad (29)$$

²i.e., there is no pair $v \in \mathbb{R}^n$, $c \in \mathbb{R}$ such that $\langle X, v \rangle = c$, almost surely.

where ϕ_{MMSE} is as in (28) and C_{x_0} takes the form

$$C_{x_0} := \frac{1}{\sigma^2} (M_1 \phi_{\text{MMSE}}(x_0) - f_Z(x_0)), \quad (30)$$

for any choice of $x_0 \in \mathbb{R}^n$.

Proof. Pick $x \in \mathbb{R}^n$. By Theorem II.8,

$$\begin{aligned} x - \text{prox}_{\phi_{\text{MMSE}}}(x) &= -\sigma^2 \nabla \log p_Z(x) \\ &= \sigma^2 \nabla f_Z(x), \end{aligned} \quad (31)$$

which gives us

$$\sigma^2 \nabla f_Z(x) = \nabla M_1 \phi_{\text{MMSE}}(x), \quad (32)$$

when combined with Theorem II.7. Integrating gives the result. \square

Theorem III.2. *The regularizer implicit in the MMSE denoiser can be written as*

$$\phi_{\text{MMSE}}(x) = \sigma^2 M \sigma^2 f_Z(x) - \sigma^2 C_{x_0}, \quad (33)$$

for all x in the image of ψ_σ .

Proof. Pick some $x \in \mathbb{R}^n$. By Lemma II.5,

$$\phi_{\text{MMSE}}(x) \geq M^1 M_1 \phi_{\text{MMSE}}(x), \quad (34)$$

which, by the previous result, we can rewrite as

$$\begin{aligned} \phi_{\text{MMSE}}(x) &\geq M^1 (\sigma^2 f_Z - \sigma^2 C_{x_0})(x) \\ &= \sigma^2 M \sigma^2 f_Z(x) - \sigma^2 C_{x_0}. \end{aligned} \quad (35)$$

For the reverse inequality, take some x in the image of ψ_σ . There exists some $z \in \mathbb{R}^n$ so that $x = \psi_\sigma(z) = \text{prox}_{\phi_{\text{MMSE}}}(z)$. The infimum defining $M_1 \phi_{\text{MMSE}}$ is achieved at x (see (18)), so that

$$\begin{aligned} \phi_{\text{MMSE}}(x) + \frac{1}{2} \|x - z\|^2 &= M_1 \phi_{\text{MMSE}}(z) \\ &= \sigma^2 f_Z(z) - \sigma^2 C_{x_0}, \end{aligned} \quad (36)$$

where the second line holds by Lemma III.1. Rearranging, we have

$$\begin{aligned} \phi_{\text{MMSE}}(x) &= \sigma^2 (f_Z(z) - \frac{1}{2\sigma^2} \|x - z\|^2) - \sigma^2 C_{x_0} \\ &\leq \sigma^2 M \sigma^2 f_Z(x) - \sigma^2 C_{x_0}. \end{aligned} \quad (37)$$

\square

We illustrate this result in Fig. 1 and Fig. 2 under a variety of mixture of Gaussian and mixture of Laplacian priors. An overview of the experiment is provided in Section IV-A.

Corollary III.3. *The regularizer ϕ_{MMSE} implicit in the MMSE denoiser is 1-weakly convex on the image of ψ_σ .*

Proof. From Theorem III.2,

$$\begin{aligned} \phi_{\text{MMSE}} &= \sigma^2 M \sigma^2 f_Z - \sigma^2 C_{x_0} \\ &= M^1 (\sigma^2 (f_Z - C_{x_0})) = M^1 M_1 \phi_{\text{MMSE}}, \end{aligned} \quad (38)$$

by Lemma III.1. This holds only if ϕ_{MMSE} is 1-weakly convex by Lemma II.5. \square

We now leverage this 1-weak convexity to derive nonasymptotic guarantees for PnP-PGD.

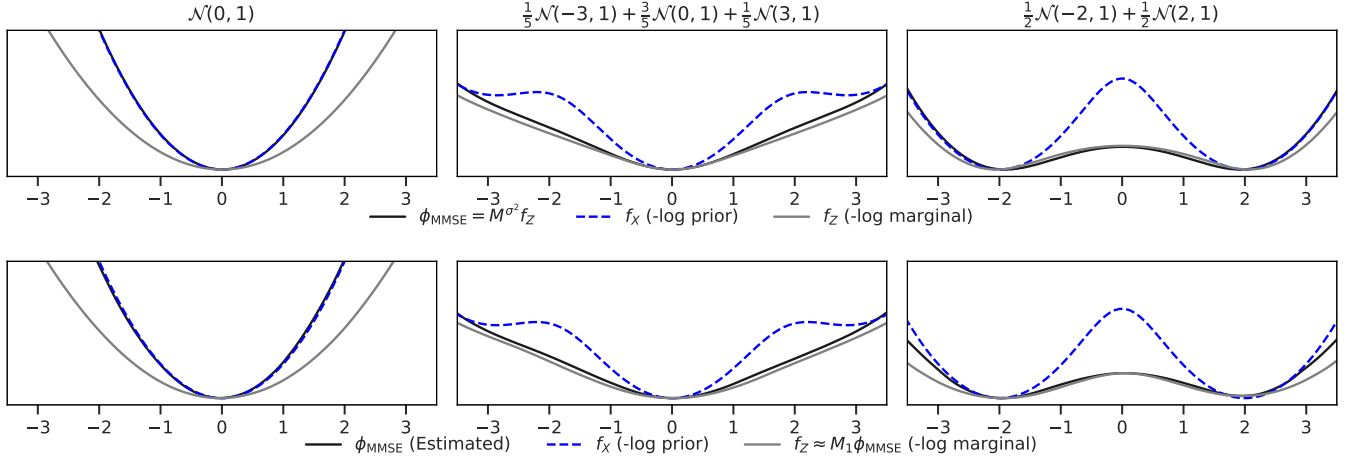


Fig. 1. Calculated and learned regularizers for an MMSE denoiser under mixture-of-Gaussian priors with unit Gaussian noise. The calculated regularizer is derived via Theorem III.2.

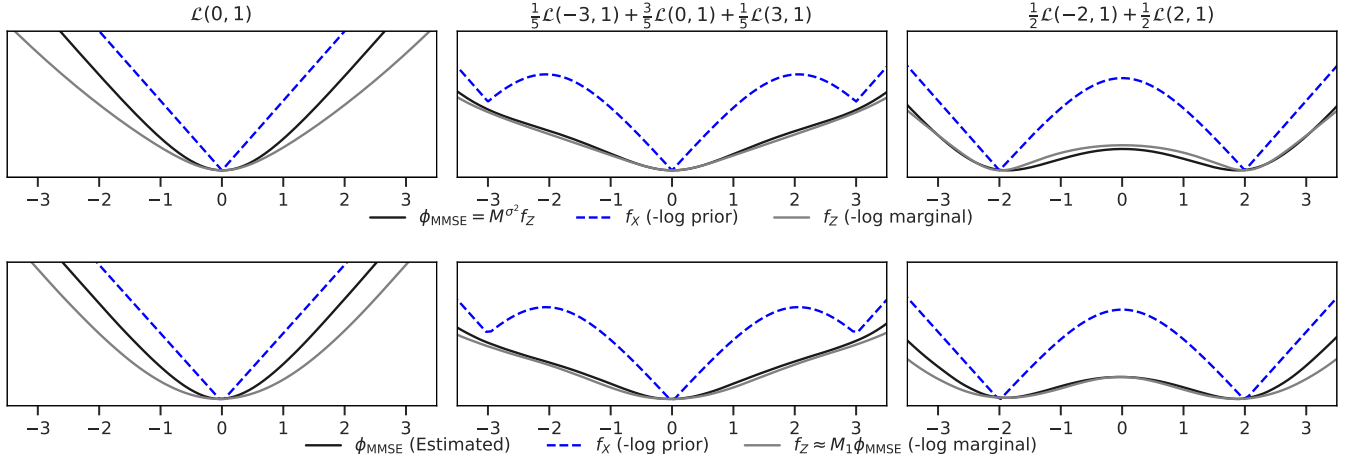


Fig. 2. Calculated and learned regularizers for an MMSE denoiser under mixture-of-Laplacian priors with unit Gaussian noise. The calculated regularizer is derived via Theorem III.2.

B. Proximal Gradient Descent Convergence Results.

When the objective F is smooth, the map $x \mapsto \nabla F(x)$ is continuous. Therefore, measuring convergence via the gradient norm $\|\nabla F(x_k)\|$ is natural; small gradient norms certify proximity to a stationary point. In the non-smooth, non-convex setting, the gradient may not exist and is generalized to the subgradient [51, Chapter 8].

Definition III.4 (Subgradient). For a function $F : \mathbb{R}^n \rightarrow \mathbb{R} \cup \{+\infty\}$, the subgradient $\partial F(x)$ is given by

$$\partial F(x) := \left\{ v \in \mathbb{R}^n \mid \begin{array}{l} F(y) \geq F(x) + \langle v, y - x \rangle, \\ \text{for all } y \in \mathbb{R}^n \end{array} \right\} \quad (39)$$

Recall that x^* is a stationary point for F if and only if $0 \in \partial F(x^*)$. This motivates measuring progress by *approximate*

stationarity. In the nonsmooth, non-convex setting, the natural goal is to find an ε -stationary point, i.e. an x satisfying

$$\text{dist}(0, \partial F(x)) \leq \varepsilon, \quad (40)$$

where

$$\text{dist}(0, \partial F(x)) := \min_{v \in \partial F(x)} \|v\|. \quad (41)$$

In non-convex, nonsmooth problems, the *stationary residual* (41) may oscillate, even while it trends downward. This can depend on the forward operator as well as the data. To account for this behavior, nonasymptotic convergence results are typically stated in terms of the best iterate *so far*. See for example [2]. It is standard to state that an algorithm *reaches* an ε -stationary point in the first k iterations if

$$\min_{1 \leq j \leq k} \text{dist}(0, \partial F(x_j)) \leq \varepsilon. \quad (42)$$

For our investigation, we prove the following intermediary result, which is a simple improvement over [5, Theorem 5.1].

This result will be used to prove convergence of PGD using an MMSE denoiser.

Lemma III.5. *Let $\{x_k\}$ be iterates of proximal gradient descent defined in (5), where g is proper, lower-semicontinuous, ρ -weakly convex, and ∇f is L -Lipschitz continuous. Suppose $\gamma \in \left(0, \frac{2}{L+\rho}\right)$. Then, for all $k \geq 1$,*

$$\min_{2 \leq j \leq k+1} \text{dist}(0, \partial F(x_j)) \leq k^{-1/2} C \sqrt{F(x_1) - F^*}, \quad (43)$$

where F is as in (3),

$$F^* := \liminf_{k \rightarrow \infty} F(x_k), \quad (44)$$

and

$$C = \frac{\frac{1}{\gamma} + L}{\sqrt{\frac{1}{\gamma} - \frac{L+\rho}{2}}}. \quad (45)$$

In other words, there is an ϵ -stationary point in the first $k+1$ iterates with $\epsilon \sim \mathcal{O}(1/\sqrt{k})$.

Proof. We first note that $\tilde{g}(x) := g(x) + \frac{\rho}{2}\|x\|^2$ is convex, so

$$\tilde{g}(y) \geq \tilde{g}(x) + \langle s, y - x \rangle, \quad (46)$$

for any $s \in \partial \tilde{g}(x)$. For iteration x_{k+1} , let $s_{k+1} \in \partial g(x_{k+1})$, so that $s_{k+1} + \rho x_{k+1} \in \partial \tilde{g}(x_{k+1})$. We then have

$$\begin{aligned} g(x_k) + \frac{\rho}{2}\|x_k\|^2 &\geq g(x_{k+1}) + \frac{\rho}{2}\|x_{k+1}\|^2 \\ &\quad + \langle s_{k+1} + \rho x_{k+1}, x_k - x_{k+1} \rangle, \end{aligned} \quad (47)$$

using (46) with $y = x_k$, $x = x_{k+1}$, and $s = s_{k+1} + \rho x_{k+1}$. We will write this as

$$\begin{aligned} g(x_k) &\geq g(x_{k+1}) + \langle s_{k+1}, x_k - x_{k+1} \rangle \\ &\quad - \frac{\rho}{2}\|x_k - x_{k+1}\|^2. \end{aligned} \quad (48)$$

∇f is L -Lipschitz, so

$$\begin{aligned} f(x_{k+1}) &\leq f(x_k) + \langle \nabla f(x_k), x_{k+1} - x_k \rangle \\ &\quad + \frac{L}{2}\|x_{k+1} - x_k\|^2. \end{aligned} \quad (49)$$

Setting $s_{k+1} := \frac{1}{\gamma}(x_k - x_{k+1}) - \nabla f(x_k) \in \partial g(x_{k+1})$ and adding (48) and (49),

$$\left(\frac{1}{\gamma} - \frac{L+\rho}{2}\right)\|x_k - x_{k+1}\|^2 \leq F(x_k) - F(x_{k+1}). \quad (50)$$

Next, let $w_{k+1} := \frac{1}{\gamma}(x_{k+1} - x_k) + \nabla f(x_{k+1}) - \nabla f(x_k)$, an element of $\partial(f+g)(x_{k+1})$,

$$\begin{aligned} \|w_{k+1}\|^2 &\leq \left(\frac{1}{\gamma} + L\right)^2 \|x_{k+1} - x_k\|^2 \\ &\leq C^2(F(x_k) - F(x_{k+1})), \end{aligned} \quad (51)$$

by (50), where $C = \frac{\frac{1}{\gamma} + L}{\sqrt{\frac{1}{\gamma} - \frac{L+\rho}{2}}}$. Next, we have a simple telescoping sum,

$$\begin{aligned} \min_{1 \leq j \leq k} \|w_{j+1}\|^2 &\leq \frac{1}{k} \sum_{j=1}^{k+1} \|w_j\|^2 \\ &\leq \frac{1}{k} C^2(F(x_1) - F(x_{k+1})) \\ &\leq C^2(F(x_1) - F^*), \end{aligned} \quad (52)$$

using the definition in (44). Taking a square root and recalling that $\text{dist}(0, \partial F(x_{j+1})) \leq \|w_{j+1}\|$ gives us the result. \square

Convergence of PGD using an MMSE denoiser has been previously established for a range of step sizes $\gamma > 0$. In particular, [59] showed that PnP-MMSE converges for any $\gamma \leq 1/L$, but the objective it converges to is not the objective of interest, i.e.,

$$F(x) = f(x) + \phi_{\text{MMSE}}(x), \quad (53)$$

but instead it converges to a *scaled objective* of the form

$$F(x) = f(x) + \frac{1}{\gamma} \phi_{\text{MMSE}}(x). \quad (54)$$

Furthermore, their convergence is only asymptotic. On the other hand, in this paper, we establish a nonasymptotic convergence result for the objective (53). Our result is summarized in the following theorem.

Theorem III.6. *Consider the PnP iteration (6) using $D_\sigma := \psi_\sigma$, the MMSE denoiser with implicit step size $\gamma = 1$. If ∇f is L -Lipschitz continuous with $L < 1$, there exists an $\mathcal{O}(1/\sqrt{k})$ -stationary point among $\{x_j\}_{j=1}^{k+1}$.*

Proof. Apply Lemma III.5 with $\rho = 1$, since ϕ_{MMSE} is 1-weakly convex. Note that the iterates x_j lie in the image of ψ_σ for $j \geq 2$, so Theorem III.2 applies to them. \square

IV. EXPERIMENTS

A. Illustration of Theorem III.2.

We consider the denoising problem (2) under mixture-of-Gaussian and mixture-of-Laplacian priors with unit Gaussian noise. We train a gradient-output softplus input convex neural network (ICNN) to approximate the MMSE denoiser and calculate its implicit prior via [26, Theorem 3]. We compare this with the implicit regularizer calculated using the explicit upper Moreau envelope formula from Theorem III.2. Figures 1 and 2 compare the calculated ϕ_{MMSE} and the learned estimate, along with reference curves $f_X := -\log p_X$ and $f_Z := -\log p_Z$. The learned and calculated regularizers are nearly identical where the samples are most concentrated.

We observe that the learned implicit regularizer ‘‘curls downward’’ outside the central region of the data. This behavior is intrinsic to ReLU-based neural networks (and their softplus approximations). It is well known that feedforward networks with continuous piecewise-affine activations yield continuous piecewise-affine mappings [39], [49]. The ReLU is piecewise-affine and is the uniform limit of the softplus family. Thus, an ICNN with softplus activations is a smooth approximation of a ReLU-ICNN and is therefore nearly piecewise-affine.

Outside the support of the training data, the learned convex potential becomes approximately affine, and its gradient (the denoiser) saturates. To solve for $\phi_{\text{MMSE}}(x)$, we must invert the learned denoiser numerically. This inversion is impossible where the denoiser saturates, so we get large values for ψ_θ^{-1} outside the central region. We solve for $\phi_{\text{MMSE}}(x)$ using [26, Eq. (8)], so the quadratic $-g_\theta(\psi_\theta^{-1}(x))$ dominates, causing the resulting estimate of the regularizer to curl downward to $-\infty$. We emphasize that this behavior arises as a result of the

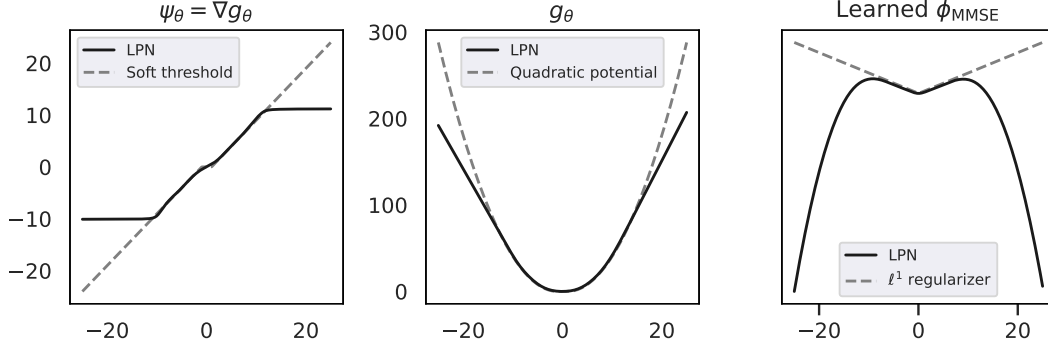


Fig. 3. MMSE denoiser, convex potential, and implicit MMSE regularizer for a Laplacian prior $p_X(x) = e^{-|x|}$, plotted against reference curves. LPN denotes the learned proximal network. This explicates what is shown in [22, Figure 2], but plotted on a wider axis to show the “curling down” behavior of LPNs.

ReLU-approximating architecture, not from the MMSE loss or our implementation. To illustrate this, in Figure 3 we reproduce the setup of [22, Fig. 2] and simply extend the axis range. The extended view makes the affine-tail/saturation effect apparent.

B. Gaussian Blurring.

We next consider PGD for the Gaussian blurring inverse problem (1), where X is sampled from the MNIST data set of handwritten digits [34] (resolution of 28×28). A is a Gaussian blurring operator, computed by convolution with a 3×3 Gaussian kernel with $\sigma^2 = 1$, and measurement noise ϵ being a zero-mean standard Gaussian with variance $\sigma^2 = 0.04$. The Gaussian kernel has unit mass, giving the blur an operator norm $\|A\|_{\text{op}} = 1$.

We use data-fidelity term $f(x) := \frac{1}{2}\|Ax - y\|^2$ normalized to have $L < 1$. We use an MMSE denoiser trained with noise $\sigma^2 = 0.04$ for the proximal step. We confirm the efficacy of this algorithm on 5 test examples in Figure 4. At this noise level, the observed blurry images have a PSNR of ≈ 15 dB, while the reconstructions reach PSNR of ≈ 20 dB.

In Figure 5, we plot $\text{dist}(0, \partial F(x_k))$ over 50 iterations for the first test image in Figure 4, showing clear sublinear fixed-point convergence, as predicted by Theorem III.6.

C. Computed Tomography.

We study the CT inverse problem with forward operator A given by the discretized Radon transform, normalized to $\|A\|_{\text{op}} < 1$. Training images are random 128×128 patches sampled from the MayoCT dataset [37] (resolution of 512×512).

We test the PGD algorithm using the MMSE denoiser on randomly selected regions of the Shepp–Logan phantom [54], which captures a wide range of structures relevant in computed tomography. We corrupt measurements with zero-mean Gaussian noise to yield input PSNR levels of 20, 24, and 28 dB, ranges commonly studied for low-dose CT (LDCT). See for example [61, Table 6]. After 5 iterations of PGD we obtain reconstructions in the range of 37–38 dB which we display in Figs. 6 and 7.

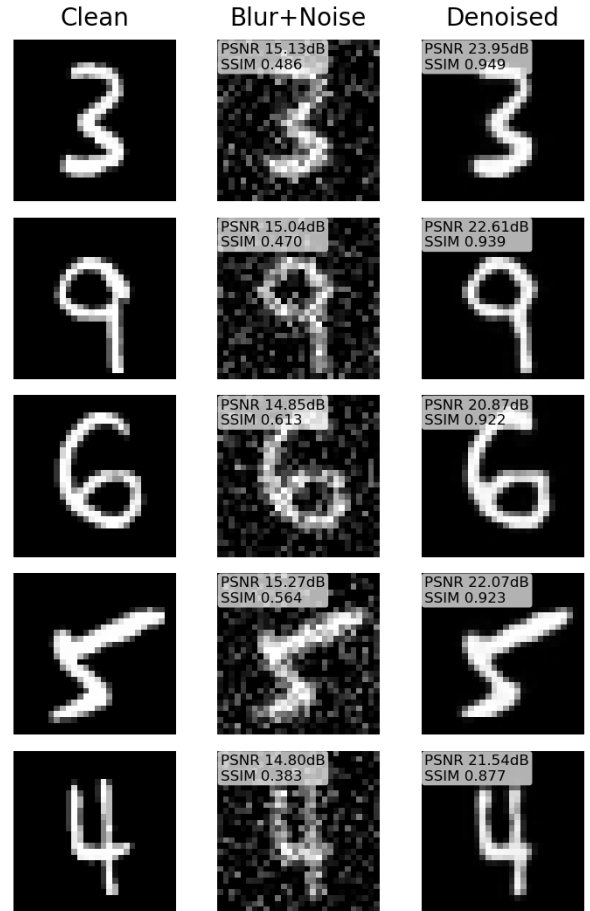


Fig. 4. PNP-PGD results on the MNIST dataset under Gaussian blur.

In Fig. 8, we plot the stationary residual (41) for 160 iterations and observe behavior consistent with our findings in Theorem III.6

D. Architectural Details.

We build upon the implementation of the Input Convex Neural Network (ICNN) in [22] to approximate the MMSE

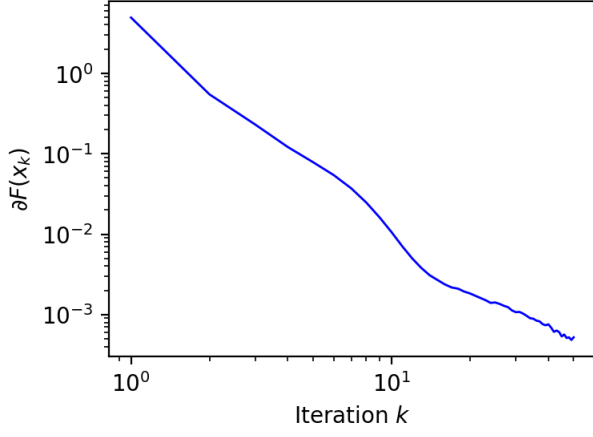


Fig. 5. Stationary residual (41) over 50 iterations for PnP-PGD using an MMSE denoiser on the MNIST dataset under Gaussian blur.

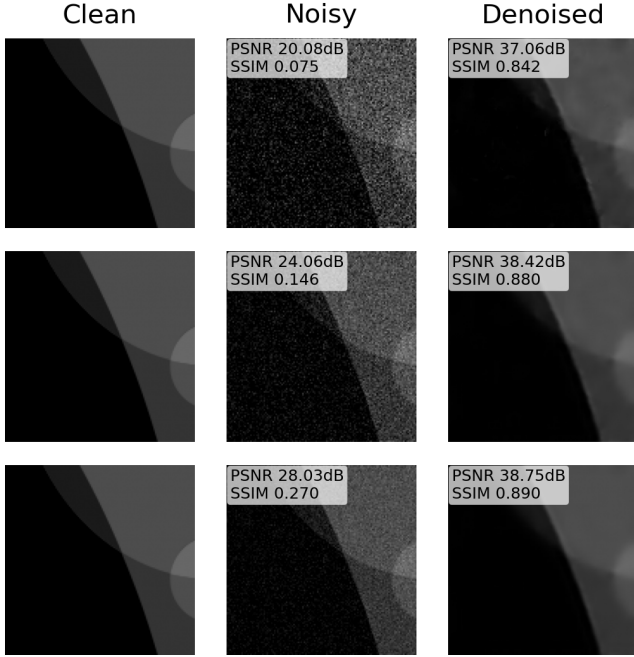


Fig. 6. Randomly selected 128×128 region of the Shepp-Logan phantom. Clean, noisy/blurred, and PnP-PGD reconstruction with an MMSE denoiser after 5 iterations. Gaussian noise; per-panel PSNR/SSIM are denoted.

denoiser. The authors produced excellent results with softplus activations and a mixture of linear and convolutional layers.³ The network uses layers of the form

$$h_0 = \sigma(A_0x + b_0), \quad (55)$$

$$h_{k+1} = \sigma(W_{k+1}h_k + A_{k+1}x + b_{k+1}), \quad (56)$$

with hidden layers $W_k \in \mathbb{R}^{H \times H}$, skip connections $A_k \in \mathbb{R}^{H \times H}$, and softplus activation $\sigma(x) = \frac{1}{\beta} \log(1 + \exp(\beta x))$ applied element-wise ($\beta = 10$). Softplus is a differentiable

³The exact PyTorch implementation is available at <https://github.com/ZhenghanFang/learned-proximal-networks>

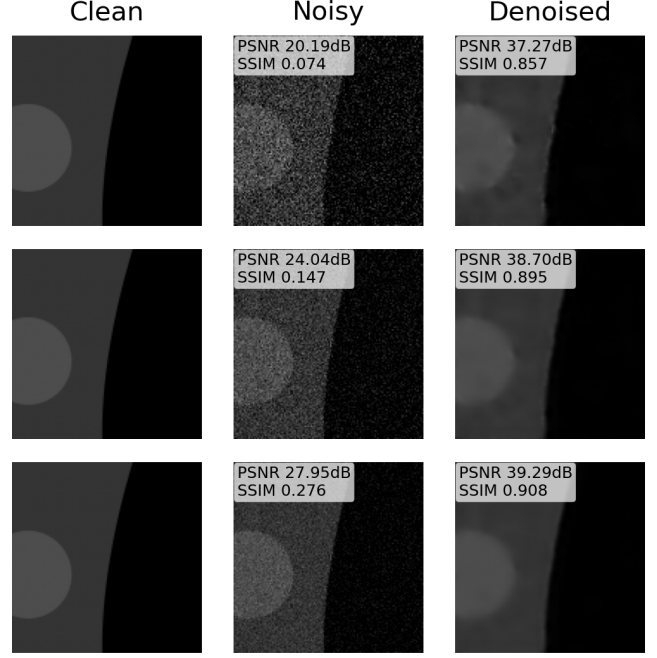


Fig. 7. Randomly selected 128×128 region of the Shepp-Logan phantom. Clean, noisy/blurred, and PnP-PGD reconstruction with an MMSE denoiser after 5 iterations. Gaussian noise; per-panel PSNR/SSIM are denoted.

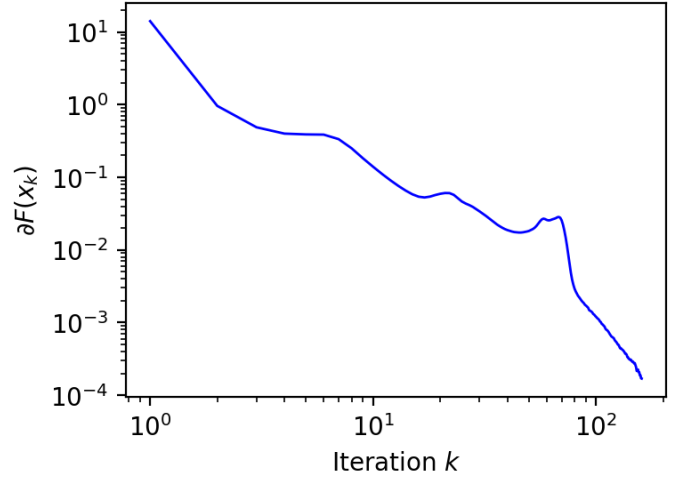


Fig. 8. Stationary residual (41) over 160 iterations for PnP-PGD on the MayoCT dataset using an MMSE denoiser.

approximation of ReLU, so that the denoiser can be defined as the gradient $\psi_\theta := \nabla g_\theta$ of potential $g_\theta : \mathbb{R}^n \rightarrow \mathbb{R}$ given by

$$g_\theta(x) := w_{\text{out}}^T h_L + a_{\text{out}}^T x + b_{\text{out}}. \quad (57)$$

To ensure convexity in x , all hidden layers W_k are clipped so that they have only non-negative entries. Note that a convolutional layer can be represented as a matrix. For the MayoCT and MNIST experiments, the hidden layers are clipped in this form, not in kernel form. Because the activation is convex and non-decreasing, these constraints make g_θ convex,

guaranteeing that its gradient (ψ_θ) is a proximal operator [26, Corollary 1]. Note that no restrictions on the skip-connections or biases are necessary.

E. Training Details.

For the illustration of Theorem III.2, the data was divided into batches of 4,000 with 2,000 iterations at learning rate 10^{-3} . For Gaussian deblurring, the dataset was divided into batches of 500 with noise of $\sigma^2 = 0.04$. The training schedule is detailed in Table I. For computed tomography, the dataset was

TABLE I
MNIST AND MAYOCT DENOISER LEARNING-RATE SCHEDULE

Phase	Learning rate	Steps
1	1×10^{-3}	10,000
2	3×10^{-4}	15,000
3	1×10^{-4}	10,000
4	3×10^{-5}	5,000

divided into batches of 64 with noise level of $\sigma^2 = 0.01$. The forward operator was implemented using the ODL⁴ Python library and normalized to have operator norm $\|A\|_{op} < 1$. Training examples were identical to Table I. All training and testing was done on an Nvidia 4070 GPU using the Ubuntu 24.04 Windows Subsystem for Linux.

Remark IV.1. We note that while the restriction of $L < 1$ in Theorem III.6 may seem potentially restrictive, any L -smooth data-fidelity term can be scaled appropriately to meet this condition. For example, in our computed tomography experiment, the forward operator, a discretized Radon transform is L -smooth with $L \approx 450$. We simply scale the data fidelity term appropriately and still obtain strong empirical results with the desired convergence rate.

V. CONCLUSION

We presented a novel representation of the MMSE denoiser’s implicit regularizer in Theorem III.2 and used it to derive nonasymptotic convergence results for PnP-PGD using an MMSE denoiser in Theorem III.6. Our analysis is strictly tied to the Gaussian-noise MMSE setting. Tweedie’s formula, for example, does not transfer to other noise models, so we suspect this flavor of result is unique to the Gaussian noise setting. However, we expect analogous nonasymptotic guarantees to be attainable for other PnP schemes that use MMSE denoisers under Gaussian noise, such as PnP-ADMM or the proximal point method. Exploration of these extensions constitutes future work toward more predictable PnP solvers.

ACKNOWLEDGMENT

The authors would like to thank Stanislas Ducotterd for helpful feedback on this work.

⁴Documentation available at <https://odlgroup.github.io/odl/>.

REFERENCES

- [1] R. Ahmad, C. A. Bouman, G. T. Buzzard, S. Chan, S. Liu, E. T. Reehorst, and P. Schniter, “Plug-and-play methods for magnetic resonance imaging: Using denoisers for image recovery,” *IEEE signal processing magazine*, vol. 37, no. 1, pp. 105–116, 2020.
- [2] H. Attouch, J. Bolte, and B. F. Svaiter, “Convergence of descent methods for semi-algebraic and tame problems: proximal algorithms, forward-backward splitting, and regularized gauss–seidel methods,” *Mathematical programming*, vol. 137, no. 1, pp. 91–129, 2013.
- [3] H. H. Bauschke and P. L. Combettes, “Convex analysis and monotone operator theory in hilbert spaces,” *CMS Books in Mathematics, Ouvrages de mathématiques de la SMC*, 2011.
- [4] P. Bernard, “Lasry-lions regularization and a lemma of ilmanen,” *Rendiconti del Seminario Matematico della Università di Padova*, vol. 124, pp. 221–229, 2010.
- [5] A. Böhm and S. J. Wright, “Variable smoothing for weakly convex composite functions,” *Journal of optimization theory and applications*, vol. 188, no. 3, pp. 628–649, 2021.
- [6] A. Bora, A. Jalal, E. Price, and A. G. Dimakis, “Compressed sensing using generative models,” in *International conference on machine learning*. PMLR, 2017, pp. 537–546.
- [7] S. Boyd, N. Parikh, E. Chu, B. Peleato, J. Eckstein *et al.*, “Distributed optimization and statistical learning via the alternating direction method of multipliers,” *Foundations and Trends® in Machine learning*, vol. 3, no. 1, pp. 1–122, 2011.
- [8] K. Bredies, J. Chirinos-Rodriguez, and E. Naldi, “Learning firmly nonexpansive operators,” *arXiv preprint arXiv:2407.14156*, 2024.
- [9] E. Candes, J. Romberg, and T. Tao, “Robust uncertainty principles: exact signal reconstruction from highly incomplete frequency information,” *IEEE Transactions on Information Theory*, vol. 52, no. 2, pp. 489–509, 2006.
- [10] A. Chambolle, “An algorithm for total variation minimization and applications,” *Journal of Mathematical imaging and vision*, vol. 20, no. 1, pp. 89–97, 2004.
- [11] A. Chambolle and T. Pock, “A first-order primal-dual algorithm for convex problems with applications to imaging,” *Journal of mathematical imaging and vision*, vol. 40, no. 1, pp. 120–145, 2011.
- [12] S. H. Chan, X. Wang, and O. A. Elgendy, “Plug-and-play admm for image restoration: Fixed-point convergence and applications,” *IEEE Transactions on Computational Imaging*, vol. 3, no. 1, pp. 84–98, 2016.
- [13] P. L. Combettes, “Solving monotone inclusions via compositions of nonexpansive averaged operators,” *Optimization*, vol. 53, no. 5-6, pp. 475–504, 2004.
- [14] P. L. Combettes and J.-C. Pesquet, “Proximal splitting methods in signal processing,” in *Fixed-point algorithms for inverse problems in science and engineering*. Springer, 2011, pp. 185–212.
- [15] P. L. Combettes and V. R. Wajs, “Signal recovery by proximal forward-backward splitting,” *Multiscale modeling & simulation*, vol. 4, no. 4, pp. 1168–1200, 2005.
- [16] K. Dabov, A. Foi, V. Katkovnik, and K. Egiazarian, “Image denoising by sparse 3-d transform-domain collaborative filtering,” *IEEE Transactions on image processing*, vol. 16, no. 8, pp. 2080–2095, 2007.
- [17] D. L. Donoho, “Compressed sensing,” *IEEE Transactions on information theory*, vol. 52, no. 4, pp. 1289–1306, 2006.
- [18] S. Ducotterd, S. Neumayer, and M. Unser, “Learning of patch-based smooth-plus-sparse models for image reconstruction,” in *The Second Conference on Parsimony and Learning*, 2025.
- [19] S. Ducotterd and M. Unser, “Multivariate fields of experts,” *arXiv preprint arXiv:2508.06490*, 2025.
- [20] B. Efron, “Tweedie’s formula and selection bias,” *Journal of the American Statistical Association*, vol. 106, no. 496, pp. 1602–1614, 2011.
- [21] H. Engl, M. Hanke, and A. Neubauer, *Regularization of Inverse Problems*, ser. Mathematics and Its Applications. Springer Netherlands, 1996.
- [22] Z. Fang, S. Buchanan, and J. Sulam, “What’s in a prior? learned proximal networks for inverse problems,” *arXiv preprint arXiv:2310.14344*, 2023.
- [23] R. G. Gavaskar and K. N. Chaudhury, “Plug-and-play ista converges with kernel denoisers,” *IEEE Signal Processing Letters*, vol. 27, pp. 610–614, 2020.
- [24] A. Goujon, S. Neumayer, P. Bohra, S. Ducotterd, and M. Unser, “A neural-network-based convex regularizer for inverse problems,” *IEEE Transactions on Computational Imaging*, vol. 9, pp. 781–795, 2023.
- [25] R. Gribonval and P. Machart, “Reconciling ”priors” & ”priors” without prejudice?” in *Advances in Neural Information Processing Systems*, vol. 26, 2013.

- [26] R. Gribonval and M. Nikolova, "A characterization of proximity operators," *Journal of Mathematical Imaging and Vision*, vol. 62, no. 6, pp. 773–789, 2020.
- [27] R. Gribonval, "Should penalized least squares regression be interpreted as maximum a posteriori estimation?" *IEEE Transactions on Signal Processing*, vol. 59, no. 5, pp. 2405–2410, 2011.
- [28] J. Hadamard, "Sur les problèmes aux dérivées partielles et leur signification physique," *Princeton university bulletin*, pp. 49–52, 1902.
- [29] J. Hertrich, H. S. Wong, A. Denker, S. Ducotterd, Z. Fang, M. Haltmeier, Ž. Kereta, E. Kobler, O. Leong, M. S. Salehi *et al.*, "Learning regularization functionals for inverse problems: A comparative study," *arXiv preprint arXiv:2510.01755*, 2025.
- [30] S. Hurault, A. Leclaire, and N. Papadakis, "Proximal denoiser for convergent plug-and-play optimization with nonconvex regularization," in *International Conference on Machine Learning*. PMLR, 2022, pp. 9483–9505.
- [31] V. Jain and S. Seung, "Natural image denoising with convolutional networks," *Advances in neural information processing systems*, vol. 21, 2008.
- [32] S. M. Kakade, "Dimension free optimization and non-convex optimization," CSE 547 Machine Learning for Big Data Lecture Slides, University of Washington, 2018, lecture Notes, Spring 2018.
- [33] U. S. Kamilov, C. A. Bouman, G. T. Buzzard, and B. Wohlberg, "Plug-and-play methods for integrating physical and learned models in computational imaging: Theory, algorithms, and applications," *IEEE Signal Processing Magazine*, vol. 40, no. 1, pp. 85–97, 2023.
- [34] Y. LeCun, C. Cortes, and C. Burges, "Mnist handwritten digit database," 2010.
- [35] H. Li and Z. Lin, "Accelerated proximal gradient methods for nonconvex programming," *Advances in neural information processing systems*, vol. 28, 2015.
- [36] J. Liu, Y. Sun, X. Xu, and U. S. Kamilov, "Image restoration using total variation regularized deep image prior," in *ICASSP 2019-2019 IEEE International Conference on Acoustics, Speech and Signal Processing (ICASSP)*. Ieee, 2019, pp. 7715–7719.
- [37] C. McCollough, "Tu-fg-207a-04: Overview of the low dose ct grand challenge," *Medical Physics*, vol. 43, pp. 3759–3760, 06 2016.
- [38] P. Milanfar and M. Delbracio, "Denoising: a powerful building block for imaging, inverse problems and machine learning," *Philosophical Transactions A*, vol. 383, no. 2299, p. 20240326, 2025.
- [39] G. Montúfar, R. Pascanu, K. Cho, and Y. Bengio, "On the number of linear regions of deep neural networks," *Advances in neural information processing systems*, vol. 27, 2014.
- [40] J. J. Moreau, "Fonctions convexes duales et points proximaux dans un espace hilbertien," *Comptes rendus hebdomadaires des séances de l'Académie des sciences*, vol. 255, pp. 2897–2899, 1962.
- [41] J.-J. Moreau, "Proximité et dualité dans un espace hilbertien," *Bulletin de la Société mathématique de France*, vol. 93, pp. 273–299, 1965.
- [42] P. Nair, R. G. Gavaskar, and K. N. Chaudhury, "Fixed-point and objective convergence of plug-and-play algorithms," *IEEE Transactions on Computational Imaging*, vol. 7, pp. 337–348, 2021.
- [43] G. Ongie, A. Jalal, C. A. Metzler, R. G. Baraniuk, A. G. Dimakis, and R. Willett, "Deep learning techniques for inverse problems in imaging," *IEEE Journal on Selected Areas in Information Theory*, vol. 1, no. 1, pp. 39–56, 2020.
- [44] R. Parhi and M. Unser, "The sparsity of cycle spinning for wavelet-based solutions of linear inverse problems," *IEEE Signal Processing Letters*, vol. 30, pp. 568–572, 2023.
- [45] N. Parikh, S. Boyd *et al.*, "Proximal algorithms," *Foundations and trends® in Optimization*, vol. 1, no. 3, pp. 127–239, 2014.
- [46] C. Park, S. Shoushtari, W. Gan, and U. S. Kamilov, "Convergence of nonconvex pnp-admm with mmse denoisers," in *2023 IEEE 9th International Workshop on Computational Advances in Multi-Sensor Adaptive Processing (CAMSAP)*. IEEE, 2023, pp. 511–515.
- [47] J.-C. Pesquet, A. Repetti, M. Terris, and Y. Wiaux, "Learning maximally monotone operators for image recovery," *SIAM Journal on Imaging Sciences*, vol. 14, no. 3, pp. 1206–1237, 2021.
- [48] M. Pourya, E. Kobler, M. Unser, and S. Neumayer, "DEALing with image reconstruction: Deep attentive least squares," in *International Conference on Machine Learning (ICML)*, 2025.
- [49] M. Raghu, B. Poole, J. Kleinberg, S. Ganguli, and J. Sohl-Dickstein, "On the expressive power of deep neural networks," in *international conference on machine learning*. PMLR, 2017, pp. 2847–2854.
- [50] R. Rockafellar, *Convex Analysis*, 1970, vol. 28.
- [51] R. T. Rockafellar and R. J. Wets, *Variational analysis*. Springer, 1998.
- [52] L. I. Rudin, S. Osher, and E. Fatemi, "Nonlinear total variation based noise removal algorithms," *Physica D: nonlinear phenomena*, vol. 60, no. 1–4, pp. 259–268, 1992.
- [53] E. Ryu, J. Liu, S. Wang, X. Chen, Z. Wang, and W. Yin, "Plug-and-play methods provably converge with properly trained denoisers," in *International Conference on Machine Learning*. PMLR, 2019, pp. 5546–5557.
- [54] L. A. Shepp and B. F. Logan, "The fourier reconstruction of a head section," *IEEE Transactions on nuclear science*, vol. 21, no. 3, pp. 21–43, 1974.
- [55] C. Stein, "A bound for the error in the normal approximation to the distribution of a sum of dependent random variables," in *Proceedings of the sixth Berkeley symposium on mathematical statistics and probability, volume 2: Probability theory*, vol. 6. University of California Press, 1972, pp. 583–603.
- [56] Y. Sun, B. Wohlberg, and U. S. Kamilov, "An online plug-and-play algorithm for regularized image reconstruction," *IEEE Transactions on Computational Imaging*, vol. 5, no. 3, pp. 395–408, 2019.
- [57] M. Terris, A. Repetti, J.-C. Pesquet, and Y. Wiaux, "Building firmly nonexpansive convolutional neural networks," in *ICASSP 2020-2020 IEEE International Conference on Acoustics, Speech and Signal Processing (ICASSP)*. IEEE, 2020, pp. 8658–8662.
- [58] S. V. Venkatakrishnan, C. A. Bouman, and B. Wohlberg, "Plug-and-play priors for model based reconstruction," in *2013 IEEE Global Conference on Signal and Information Processing*, 2013, pp. 945–948.
- [59] X. Xu, Y. Sun, J. Liu, B. Wohlberg, and U. S. Kamilov, "Provable convergence of plug-and-play priors with mmse denoisers," *IEEE Signal Processing Letters*, vol. 27, pp. 1280–1284, 2020.
- [60] K. Zhang, W. Zuo, Y. Chen, D. Meng, and L. Zhang, "Beyond a gaussian denoiser: Residual learning of deep cnn for image denoising," *IEEE transactions on image processing*, vol. 26, no. 7, pp. 3142–3155, 2017.
- [61] H. Zhao, L. Qian, Y. Zhu, and D. Tian, "Low dose ct image denoising: A comparative study of deep learning models and training strategies," *AI Medicine*, pp. 7–7, 2024.